NANO · MICRO small
www.small-journal.com

Programmable Knot Microfibers from Piezoelectric Microfluidics

Chaoyu Yang, Yunru Yu, Xiaocheng Wang, Luoran Shang, and Yuanjin Zhao**

Microfibers have demonstrated significant application values in a large number of areas. Current efforts focus on developing new technologies to prepare microfibers with controllable morphological and structural features to enhance their functions. Here, a piezoelectric microfluidic platform is presented for consecutive spinning of functional microfibers with programmable spindle-knots. In this platform, a jet of a pregel-solution flowing in the channel can be subjected to a programmable piezoelectric signal and vibrates synchronously. Following a rapid polymerization of the wavy jet, microfibers with corresponding morphologies can be generated, including uniform, gradient, and symmetrical knots. Such a unique knot structure contributes to a water-collection mechanism. Thus, it has been observed that microfibers with programmed knots enable even more flexible droplet handling and active water transport. In addition, by constructing higher-order knot fiber networks, practical applications including spray reaction, lab-on-a-chip vapor detection, etc., can also be demonstrated. it is believed that this platform opens a new avenue for fiber spinning, and the programmable microfibers would be highly applicable in chemical, biomedical, and environmental areas.

1. Introduction

Microfibers are spectacular materials that have been extensively applied in daily life since ancient times.[1,2] More intriguingly, microfibers play an indispensable role in the life process of many organisms, such as silk fibers produced by silkworms and spiders.[3,4] Some of the natural microfibers even possess extraordinary properties including mechanical strength, moisture ability, and biocompatibility.[5,6] These metrics benefit from the highly-specialized generation process, which relies on sophisticated spinning glands to continuously transform soluble proteins into solid microfibers.[7] Inspired by this, various techniques have been developed to construct artificial microfibers including dry-spinning, wet-spinning, electrospinning, direct writing, etc.[8–12] The resultant microfibers have demonstrated their values in biomedical, energy converting, and environmental engineering areas.[13–17] Although great progress has been achieved, the current spinning methods are mostly limited to the generation of uniform fibers, while it remains difficult in constructing fibers with tailorable configurations that surpass the natural fibers.

In this paper, we proposed a piezoelectric microfluidic strategy for generating microfibers with programmable knotted structures, as illustrated in **Figure 1**a. Microfluidics is a technique enabling precise and systematic processing of individual fluids in microscale channels.[18–25] Due to this capacity, it has been widely used in continuous spinning of microfibers with straight, spiral, Janus, and multicompartmental geometries.[26–30] In particular, by combining with an on-chip emulsification process, the microfibers could be endowed with a unique spindle-knot structure, whose heterogeneous shape contributes to the functions of water collection and droplet manipulation.[31–37] However, due to the lack of programmability in the fluid dynamics,

C. Yang, Y. Zhao
Department of Clinical Laboratory
The Affiliated Drum Tower Hospital of Nanjing
University Medical School
Nanjing 210008, China

C. Yang, L. Shang
Shanghai Xuhui Central Hospital
Zhongshan-Xuhui Hospital and the Shanghai Key Laboratory of Medical Epigenetics the International Co-laboratory of Medical Epigenetics, and Metabolism (Ministry of Science and Technology) Institutes of Biomedical Sciences
Fudan University
Shanghai 200032, China
E-mail: luoranshang@fudan.edu.cn

The ORCID identification number(s) for the author(s) of this article can be found under https://doi.org/10.1002/smll.202104309.

DOI: 10.1002/smll.202104309

C. Yang, Y. Yu, X. Wang, Y. Zhao
Oujiang Laboratory (Zhejiang Lab for Regenerative Medicine, Vision and Brain Health)
Wenzhou, Zhejiang 325001, China

C. Yang, Y. Yu, X. Wang, L. Shang, Y. Zhao
Wenzhou Institute
University of Chinese Academy of Sciences
Wenzhou 325001, China

Y. Zhao
State Key Laboratory of Bioelectronics
School of Biological Science and Medical Engineering
Southeast University
Nanjing 210096, China
E-mail: yjzhao@seu.edu.cn

Y. Zhao
State Key Laboratory of Molecular Engineering of Polymers
Fudan University
Shanghai 200438, China

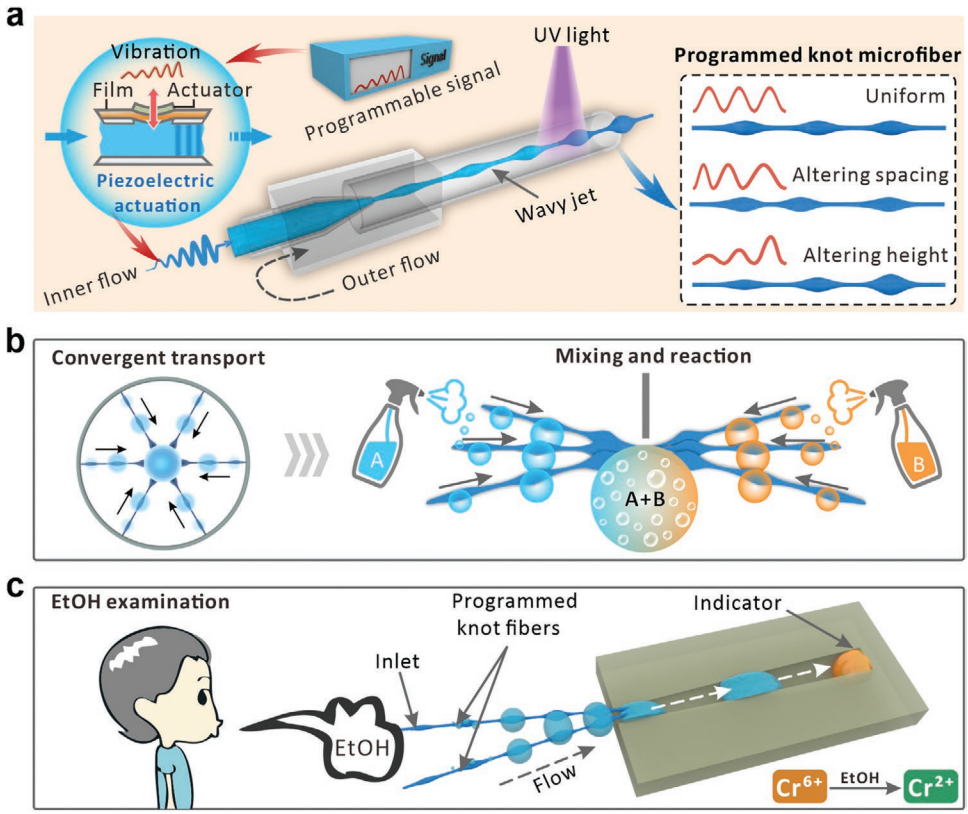

Figure 1. Schematic illustrations of the generation and application of the programmable knot microfiber. a) Schematic illustration of the piezoelectric microfluidic spinning platform. A piezoelectric actuator is applied to the inner fluid which transmits a time-variant oscillation signal to the jet flow. The jet flow vibrates synergistically and then solidifies upon ultraviolet (UV) irradiation, which results in the formation of knot fibers. The inset image shows various programmable knot fibers in response to different piezoelectric signals; b) schematic of water convergent transportation and spray reaction on a gradient microfiber network with an intersectional geometry; c) schematic figure of an EtOH vapor detection chip with the programmable gradient fibers serving as the fluid inlet. EtOH mist could be captured, and droplets could be induced to the chip and initiate a reaction with a color-changing readout.

the shape of microfluidic-spun fibers is solely constrained by the cross-sectional channel geometry and lacks diversity. Non-uniform or gradient shape fibers remain elusive and are worth studying for various potential applications.

Herein, we employed a piezoelectric microfluidic system for the generation of knot microfibers with programmable shapes. In this platform, a fluid jet of a pre-gel solution flowed in a microfluidic channel and was subjected to a piezoelectric vibration. The fluid interface oscillated synergistically to form a wavy jet, which could be converted into solid microfibers by in-situ polymerization. Benefiting from the ultrafast response of the jet to the piezoelectric signal, the resultant microfibers exhibited a unique spindle-knotted structure. Besides, by tuning the piezoelectric and microfluidic parameters of the system, the microfibers could be endowed with programmable configurations including uniform, gradient, and symmetrical knots. Due to their axially non-uniformity, the knot microfibers were demonstrated flexible capabilities in water collection, as well as unidirectional/bidirectional droplet transport. In addition, by weaving the knot fibers into patterned networks, functional devices could be constructed that achieved convergent droplet transport, spray reaction, and vapor detection (Figure 1b,c). These results indicated that the piezoelectric microfluidic technique was with unprecedented abilities in the spinning of programmable microfibers, which shed new light on application areas including droplet manipulation, water collection, and lab-on-a-chip, etc.

2. Results and Discussion

In a typical experiment, a capillary microfluidic device was constructed by coaxially aligning two cylindrical capillaries (Figure S1, Supporting Information). An inner fluid of aqueous PEG-diacrylate/Sodium alginate solution and an outer fluid of water were pumped into the device in the same direction and formed a co-flow regime. Due to the laminar flow of two phases, a steady jet is formed downstream of the microfluidic channel. Then, a piezoelectric actuator was connected to the device that could transmit an oscillation signal to the jet. The low interfacial tension of the aqueous-aqueous fluid system made the jet susceptible to deforming into a wavy configuration, as shown in **Figure 2**a. After fast solidification by UV irradiation, the jet was polymerized into a solid microfiber with periodic knots distributed along. Besides, the fiber could maintain the knotted structure in both hydrated and dehydrated states (Figure 2b), although it shrunk upon drying (Figure S2, Supporting Information). Because of the continuous jetting and fast polymerization, such a simple microfluidic method

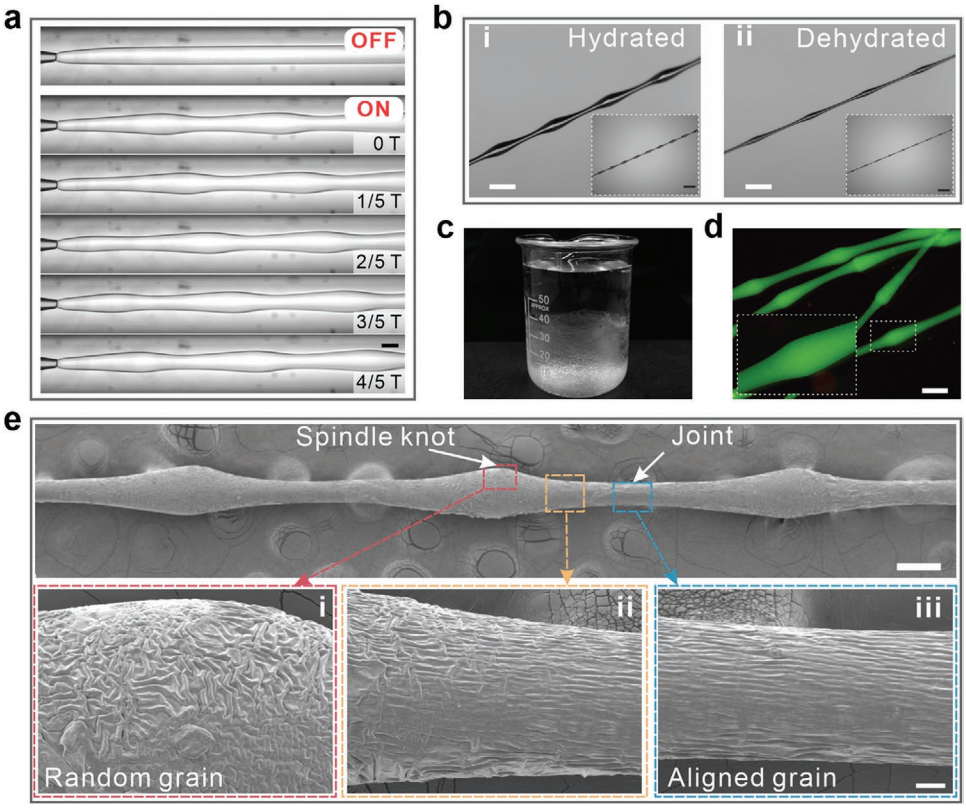

Figure 2. The jet template and characterization of knot fibers. a) Microscopic image showing a stable jet and time-lapse process of the wavy jet during one period of piezoelectric oscillation (*T*); b) microscopic image of a knot microfiber before (i) and after dehydration (ii); c) digital photograph of the collected microfibers in large quantities; d) fluorescent images of the knot microfibers, the inserted image referred to knot component homogeneity; e) SEM image of a dehydrated fiber and the magnification images of (i) the spindle knot, (ii) transition region, and (iii) joint. The scale bars are 200 µm in (a, b), 500 µm in (c), 500 µm in (e), 200 µm in the upper panel of f), and 20 µm in the bottom panels of (f).

enabled the continuous large-scale generation of microfibers (Figure 2c). To be specific, the production rate of the microfiber for a single channel was 69.78 cm min $^{-1}$ when the outer phase flow rate Q_o = 30 ml h^{-1} and 128.82 cm min^{-1} when Q_o = 100 ml h^{-1} (Figure S3, Supporting Information). It is worth mentioning that in this approach, the knot microfiber is formed through pulsation of a single jet instead of coating or encapsulation of another fluid phase. Thus, the fibers showed component homogeneity, as confirmed through fluorescence imaging (Figure 2d). It also showed that even when the fibers were tied, bent and coiled, the knots remained stable and were exempted from detachment (Figure S4, Supporting Information). We also characterized the microstructure of the knot microfibers by scanning electron microscopy (SEM). Compared with the uniform shape of the straight fiber (Figure S5, Supporting Information), the knot fiber showed a unique bumping shape with alternately distributed spindle knots and joints. Besides, the knot microfibers exhibited both curvature and roughness gradient along the axis (Figure 2e).

We then investigated the effects of the microfluidic and piezoelectric parameters on the configuration of the jet template in detail. It was found that the jet diameter, pulsing wavelength, and thickness of wave could be well controlled by changing the ratio of inner and outer flow rate Q_i/Q_o, the piezoelectric frequency *f*, and maximum voltage amplitude *U*, respectively. Especially, the jet diameter *d* rose from 109.0 to 355.9 µm with the ratio of inner and outer flow rate Q_i/Q_o increasing from 0.04 to 0.44, as the voltage and frequency were held constant at 10 V and 15 Hz, respectively (**Figure 3**a,d). The wave morphology of the microfiber could also be adjusted by changing the piezoelectric frequency *f*. It demonstrated that when Q_i/Q_o and *U* were held constant at 0.04 and 10 V, respectively, the wavelength λ significantly decreased from 2339.1 to 474.6 µm with the increasing *f* from 10 to 60 Hz (Figure 3b). These experimental data consisted of the theoretical predictions (Figure 3d,e, and Supporting Information Note 1). As Q_i/Q_o and *f* were respectively set as 0.06 and 15 Hz, the perturbation amplitude of the inner flow could be enhanced by increasing the voltage of the piezoelectric actuator (2–10 V) (Figure 3c). As a result, the wave height *h* varied from 139 to 176 µm, showing good linearity (Figure 3f). These above results indicated that by adjusting the microfluidic and piezoelectric parameters, the knot microfibers with controllable configurations could be generated on demand.

The microfiber with the knot structures was then well achieved by in situ polymerizing the jet due to the fast UV solidification. The mean diameter of the fiber was carefully adjusted by changing the Q_i/Q_o of the microfluidic system (Figure S6, Supporting Information). Moreover, by programming the period of the pulsing wave, the morphology of the

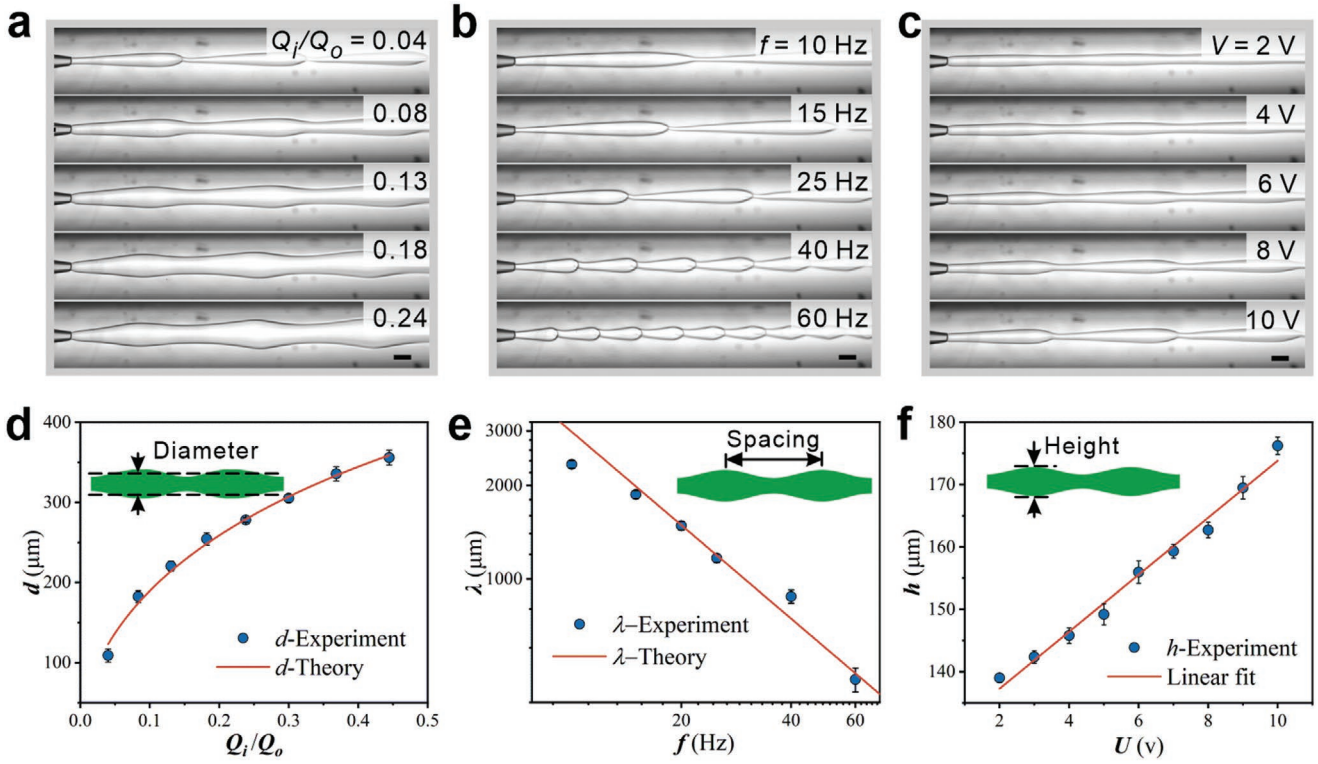

Figure 3. Microfluidic and piezoelectric parameters on the jet template. Real-time high-speed images of the dynamic behaviors of the jet under different a) the ratio of the inner and outer flow rate, b) piezoelectric actuation frequencies, and c) piezoelectric actuation amplitudes; d) plot of jet mean diameter (d) as a function of microfluidic parameters (Q_i/Q_o); e) plot of relations between jet wavelength (λ) and piezoelectric frequency (f); f) plot of relations between wave height (h) and piezoelectric amplitude (U). The scale bars are 200 μm.

microfibers could be controlled on-demand with tunable knot spacing (Figure S7, Supporting Information). At a typical set of flow rates (Q_i = 5 ml h^{-1}, Q_o = 30 ml h^{-1}), when the sinusoidal signal was induced to the inner phase, a knot fiber was formed downstream with the periodicity, as shown in **Figure 4**ai. The increasing spacing between the knots could be observed by decreasing the frequency f while fixing the amplitude (Figure 4aii). Intriguingly, the formation of microfibers with the gradient increasing spacing could be realized based on a stepwise decrease of the signal frequency, as shown in Figure 4aiii. Besides, the spacing of the knots exhibited good linearity with the pulse width (Figure 4b and Figure S8, Supporting Information). In addition, the knot height can also be programmed by modifying the signal amplitude, as illustrated in Figure S9, Supporting Information. It was easily understood that a straight microfiber formed when no external actuation was exerted, while the knotted microfiber with small knot heights could be collected when a sinusoidal signal with a lower amplitude was induced to the inner phase, as shown in Figure 4ci. One step further, when applying five intermittent amplitude gradients, the resultant microfibers showed a corresponding gradient increase in the knot size (Figure 4cii). Similarly, the symmetric knot microfibers were successfully fabricated by programming the corresponding voltage amplitudes (Figure 4ciii). To verify the controllability of the knot size, we measured the knot height of the fibers fabricated under the conditions mentioned above, and the experimental results showed a good linear relationship (Figure 4d and Figure S10, Supporting Information). The parameters used in the above experiments were summarized in Table S1, Supporting Information. It was worth noting that compared with traditional microfluidic spinning methods, the present system enables rapid programming of the microfibers due to the synchronous response of the jet template to the piezoelectric signal.

This excellent controllable property of the piezoelectric microfluidic system thus benefitted the fabrication of microfibers with tunable knot structures for water collection.[5] As illustrated in **Figure 5**a, hydrophilic knot fibers allow the adsorption of tiny water droplets and could transport them to the knots under the cooperation of wettability gradient force and Laplace pressure difference (Supporting Information Note 2). We confirmed this mechanism by observing the simultaneous water collection regardless of the knot spacing, as shown in Figure S11, Supporting Information. Intriguingly, a fiber with a gradient increasing knot size would result in unidirectional transport of water droplets toward the larger knot due to Laplace pressure difference and capillary adhesion force[38] (Figure 5a and Supporting Information Note 3). We demonstrated this property by putting a single dehydrated microfiber with gradient increasing knots (marked as s1, s2, s3, s4, s5, and s6) under fog. As shown in Figure 5b, water droplets were first collected in each knot, and then transported from s1 to s6, travelling a distance of $L_{tran} \approx 7.73$ mm. Specifically, the initial time before droplet condensation was defined as 0 s. After ≈11.08 s,

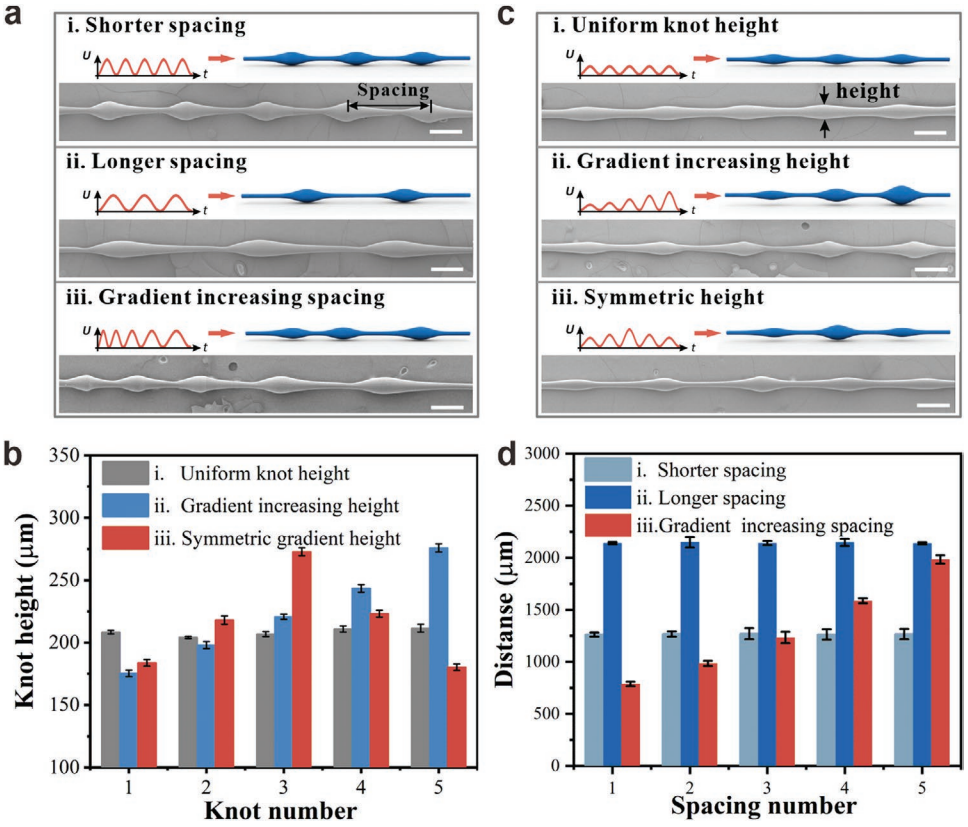

Figure 4. Programmable knot microfibers with altering spacing and height. a) Profiles of the programmed signal with editable period and corresponding SEM images of the fibers; b) measurement of the spacing of the fibers generated under conditions shown in (a); c) profiles of the programmed signal with editable amplitude and corresponding SEM images of the fibers; d) statistic records of the knot height of the fibers generated under conditions shown (c). The scale bars are 300 μm. The spacing number and the knot number are defined from left to right (the leftmost is the No. 1).

six water droplets (numbered 1, 2, 3, 4, 5, 6) were condensed on s1, s2, s3, s4, s5, and s6, respectively. Then after, the droplet 1 and 2 coalesced into one droplet (denoted as "1 + 2") at knot s2. Subsequently, the droplet 1, 2, 3, 4, and 5 coalesced into a larger droplet (denoted as "1 + 2 + 3 + 4 + 5") at ≈31.19 s at knot s5, passing knot s3 and s4. Finally, the initial six droplets coalesced into a huge droplet (denoted as "1 + 2 + 3 + 4 + 5 + 6"), hanging between the two biggest knots (s5 and s6) on the fiber at ≈32.04 s. Similarly, Figure 5c showed the droplet transport from both sides to the middle of the symmetric knot microfiber. Initially, it could be seen that each droplet that initially condensed on the knot named s1, s2, s3, respectively gradually gathered at the biggest knot in the middle (s3) and finally formed a huge droplet (denoted as "1 + 2 + 3") at ≈70.1 s. These results demonstrated that the gradient-knot microfiber allows droplets to move from small knot to big one and could thus realize long-distance directional water transport.

Based on the droplet transport ability of the programmable knot microfibers, we designed a series of devices containing assembled fiber networks for flexible droplet handling and practical applications. For example, by weaving the symmetric fibers into a radial arrangement, the size of the knots on the fiber network increased from the periphery to the center. As a result, water droplets in each fiber could move convergently toward the intersection, where all the fibers tangled together to form a huge knot with the largest water capacity (**Figure 6**a). Additionally, we fabricated a bidirectional droplet transport device composed of two convergent arrays of gradient-knot fibers for multiphase spray reaction. As shown in Figure 6b, aqueous solutions of acetic acid and baking soda were nebulized from opposite sides of the device. Because of the unidirectional convergent transportation ability of the gradient-knot fibers network on both sides, the nebulized droplets condensed, grew up, and flowed spontaneously to the intersection and eventually coalesced. Then, a metathesis reaction occurred immediately in the merged droplet to release the carbon dioxide gas product. Moreover, we constructed a self-driven lab-on-a-chip vapor detection platform where a convergent gradient-knot fiber network served as the fluidic inlet. As a proof-of-concept experiment, an ethanol (EtOH) fog flow could be captured by the gradient-knot fibers and condensed to form droplets. The droplets are then transported to the chip to mix with the indicator potassium dichromate and generate a color-changing readout, as shown in Figure 6c. These capabilities suggested that the programmable knot microfibers could be further exploited in real-life application scenarios.

3. Conclusion

In summary, we have presented a piezoelectric microfluidic platform for consecutive spinning of programmable knot

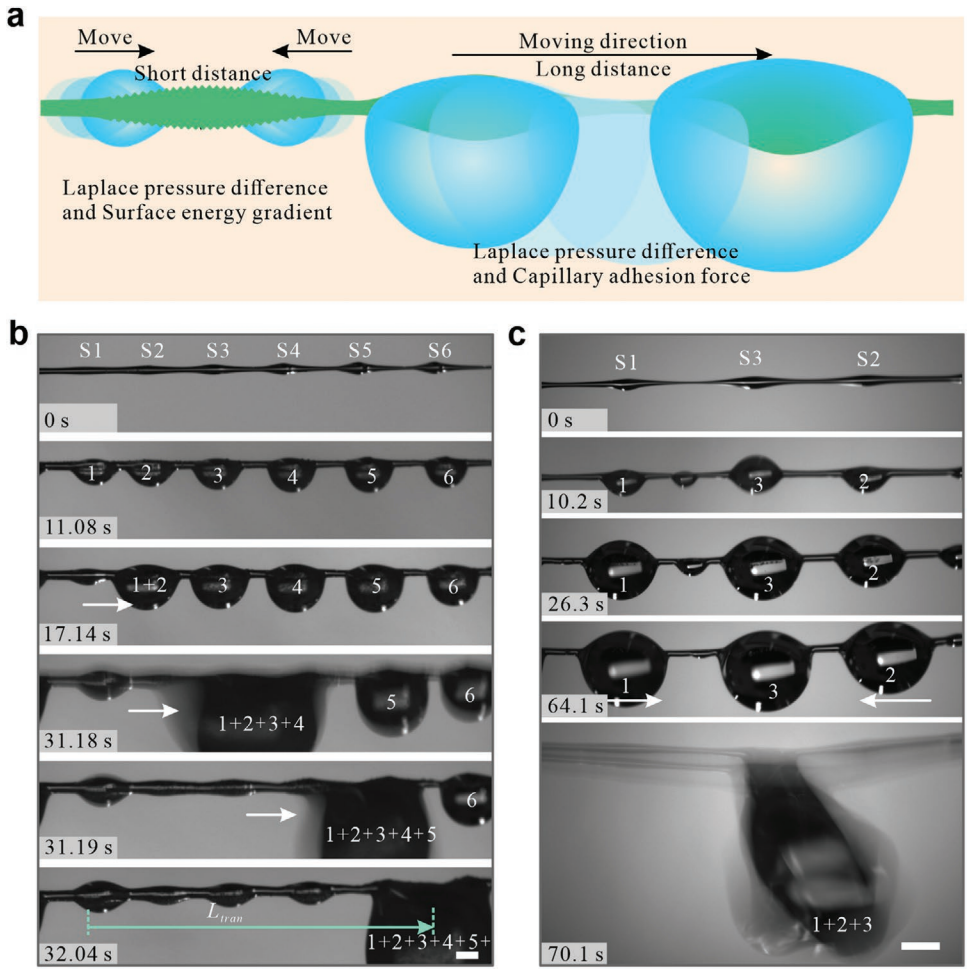

Figure 5. Long-distance directional water transport on programmable gradient knot fibers. a) Schematic illustration of the water droplet transport mechanism from the joint to the knot and from small knot to big one. b,c) Time-lapse images of droplet transportation on the (b) gradient and (c) symmetric knot fibers captured from the side view. The scale bars are 500 µm. The white arrows denote the droplets moving direction.

microfibers. The knots on the fiber were formed through pulsation of a single jet without the need of coating or encapsulation of another fluid phase. Furthermore, the diameter, knot spacing, and height of the knots were controlled synchronously by tuning the microfluidic and piezoelectric parameters. Such unique knot structure of the fiber enabled spontaneous water capture. Based on this, various arbitrary knot fibers with uniform, gradient, and symmetrical geometries were achieved by programming the piezoelectric signal, which then demonstrated flexible droplet manipulations including unidirectional/bi-directional and long-distance transport. Based on this intriguing water droplet capture and transport ability, a series of devices were proposed containing assembled fiber networks for practical applications including convergent droplet collection, spray reaction, and vapor detection. Some limitations of this study are that the formation of the wave jet depends on aqueous-aqueous fluid systems, and future endeavors can be made in developing new liquid-liquid systems with low interfacial tension, through which a large variety of functional materials could be derived. Moreover, microfluidic platforms with integrated channels (e.g., parallelized spinners) could be developed to achieve scalable preparation of programmable fibers in a higher throughput. Besides, by coupling with the 3D printing technique, macroscale entangled fiber networks with complex structures and applications could be anticipated. To further extend the potential applications of this technology, we might integrate additional components, e.g., magnetic nanoparticles, quantum dots, stimuli-responsive polymers, etc. into the hydrogel fibers. These ingredients could impart the fibers with additional functions such as controllable motion, sensing, barcoding, etc., which would appeal to applications including sensors and actuators, drug delivery, and bioassays. These results indicated that the piezoelectric microfluidic spinning platform provides a way of generating programmable knot microfibers that would find a wide range of applications in different areas.

Supporting Information

Supporting Information is available from the Wiley Online Library or from the author.

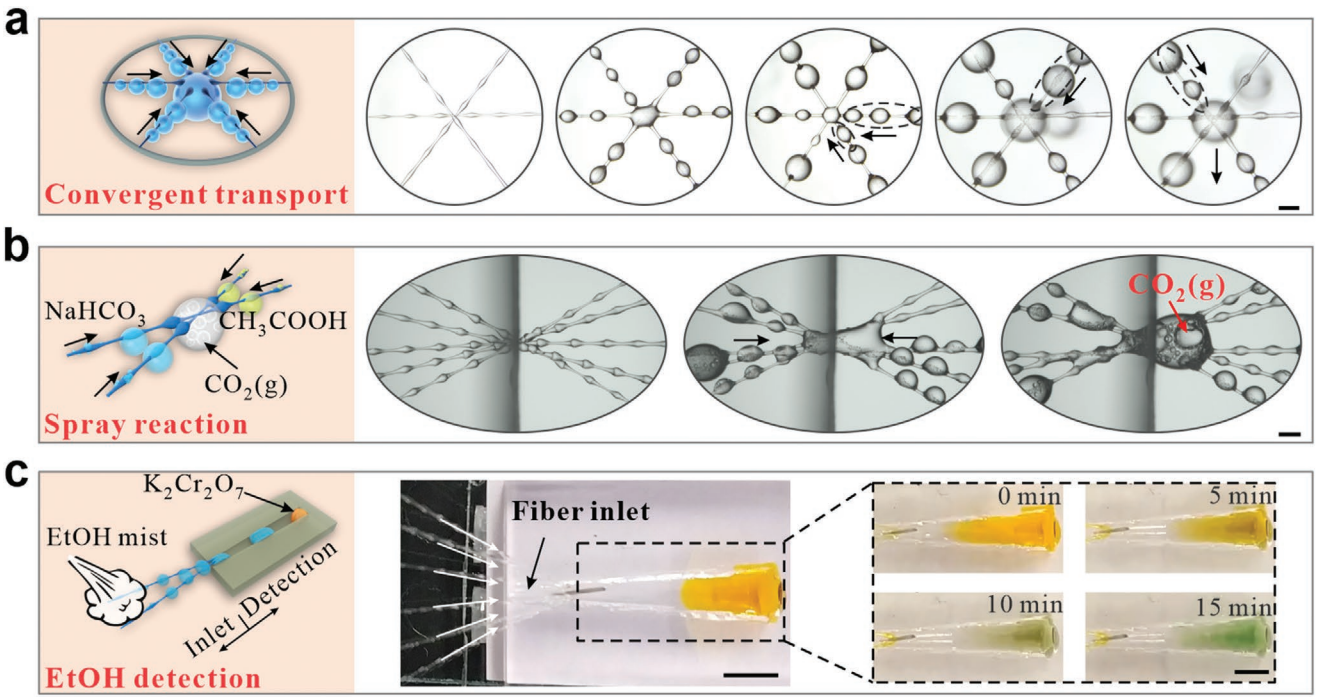

Figure 6. Programmable gradient fiber networks for flexible droplet handling and practical applications. a) Schematic figure and real-time images of the convergent droplet transport process in an intersected network of the microfibers with symmetric knots; b) schematic illustration and real-time images of the microfiber-based spray reaction process: the reaction occurred immediately after the droplets on both sides transported to the intersection; c) schematic figure and real-time images of the microfiber-based lab-on-a-chip vapor detection process: the EtOH mist was captured on the fibers and condensed to form droplets, which then transported to the chip, and the potassium permanganate indicator gradually turned to green color as it was reduced by EtOH. The scale bars are 1 mm in (a, b) and 500 µm in (c). The arrows denote the droplets moving direction.

Acknowledgements

This work was supported by the National Key Research and Development Program of China (2020YFA0908200), the National Natural Science Foundation of China (22002018, 52073060 and 61927805), the Open Foundation of the State Key Laboratory of Molecular Engineering of Polymers (K2021-08), and the Shenzhen Fundamental Research Program (JCYJ20190813152616459).

Conflict of Interest

The authors declare no conflict of interest.

Data Availability Statement

Research data are not shared.

Keywords

droplets, piezoelectric microfluidics, programmable microfibers, spindle-knot microfibers, water transportation

Received: July 21, 2021
Revised: October 1, 2021
Published online: November 25, 2021

[1] J. Yuan, W. Neri, C. Zakri, P. Merzeau, K. Kratz, A. Lendlein, P. Poulin, *Science* **2019**, *365*, 155.
[2] X. Liao, M. Dulle, J. M. d. S. e. Silva, R. B. Wehrspohn, S. Agarwal, S. Förster, H. Hou, P. Smith, A. Greiner, *Science* **2019**, *366*, 1376.
[3] W. Xin, Z. Zhang, X. Huang, Y. Hu, T. Zhou, C. Zhu, X.-Y. Kong, L. Jiang, L. Wen, *Nat. Commun.* **2019**, *10*, 3876.
[4] L. Shang, Y. Yu, Y. Liu, Z. Chen, T. Kong, Y. Zhao, *ACS Nano* **2019**, *13*, 2749.
[5] Y. Zheng, H. Bai, Z. Huang, X. Tian, F.-Q. Nie, Y. Zhao, J. Zhai, L. Jiang, *Nature* **2010**, *463*, 640.
[6] Q. Xia, Y. Guo, Z. Zhang, D. Li, Z. Xuan, Z. Li, F. Dai, Y. Li, D. Cheng, R. Li, *Science* **2009**, *326*, 433.
[7] J. Xu, Q. Dong, Y. Yu, B. Niu, D. Ji, M. Li, Y. Huang, X. Chen, A. Tan, *Proc. Natl. Acad. Sci. USA* **2018**, *115*, 8757.
[8] C. Fu, Z. Shao, V. Fritz, *Chem. Commun.* **2009**, 6515.
[9] A. Koeppel, C. Holland, *ACS Biomater. Sci. Eng.* **2017**, *3*, 226.
[10] A. Stoddart, *Nat. Rev. Mater.* **2017**, *2*, 17003.
[11] Y. S. Zhang, A. Arneri, S. Bersini, S.-R. Shin, K. Zhu, Z. Goli-Malekabadi, J. Aleman, C. Colosi, F. Busignani, V. Dell'Erba, *Biomaterials* **2016**, *110*, 45.
[12] H. Chen, Y. Zhao, Y. Song, L. Jiang, *J. Am. Chem. Soc.* **2008**, *130*, 7800.
[13] J. Cheng, Y. Jun, J. Qin, S.-H. Lee, *Biomaterials* **2017**, *114*, 121.
[14] H. Sun, Y. Zhang, J. Zhang, X. Sun, H. Peng, *Nat. Rev. Mater.* **2017**, *2*, 17023.
[15] J. Ju, Y. Zheng, L. Jiang, *Acc. Chem. Res.* **2014**, *47*, 2342.
[16] Y. Yu, J. Guo, B. Ma, D. Zhang, Y. Zhao, *Sci. Bull.* **2020**, *65*, 1752.
[17] Z. Liu, S. Fang, F. Moura, J. Ding, N. Jiang, J. Di, M. Zhang, X. Lepró, D. Galvao, C. Haines, *Science* **2015**, *349*, 400.

[18] A. K. Miri, D. Nieto, L. Iglesias, H. Goodarzi Hosseinabadi, S. Maharjan, G. U. Ruiz-Esparza, P. Khoshakhlagh, A. Manbachi, M. R. Dokmeci, S. Chen, *Adv. Mater.* **2018**, *30*, 1800242.
[19] C. Yang, R. Qiao, K. Mu, Z. Zhu, R. X. Xu, T. Si, *Phys. Fluids* **2019**, *31*, 091702.
[20] E. Kang, G. S. Jeong, Y. Y. Choi, K. H. Lee, A. Khademhosseini, S. H. Lee, *Nat. Mater.* **2011**, *10*, 877.
[21] Y. Yu, L. Shang, J. Guo, J. Wang, Y. Zhao, *Nat. Protoc.* **2018**, *13*, 2557.
[22] H. T. Liu, H. Wang, W. B. Wei, H. Liu, L. Jiang, J. H. Qin, *Small* **2018**, *14*, 1801095.
[23] X. Hou, Y. S. Zhang, G. Trujillo-de Santiago, M. M. Alvarez, J. Ribas, S. J. Jonas, P. S. Weiss, A. M. Andrews, J. Aizenberg, A. Khademhosseini, *Nat. Rev. Mater.* **2017**, *2*, 17016.
[24] Q. Pi, S. Maharjan, X. Yan, X. Liu, B. Singh, A. M. van Genderen, F. Robledo-Padilla, R. Parra-Saldivar, N. Hu, W. Jia, *Adv. Mater.* **2018**, *30*, 1706913.
[25] J. Kim, Y. Song, L. He, H. Kim, H. Lee, W. Park, Y. Yin, S. Kwon, *Small* **2011**, *7*, 1163.
[26] Y. Cheng, F. Zheng, J. Lu, L. Shang, Z. Xie, Y. Zhao, Y. Chen, Z. Gu, *Adv. Mater.* **2014**, *26*, 5184.
[27] J. K. Nunes, H. Constantin, H. A. Stone, *Soft Matter* **2013**, *9*, 4227.
[28] R. Liu, B. Kong, Y. Chen, X. Liu, S. Mi, *Sens. Actuators, B* **2020**, *304*, 127069.
[29] Y. Yu, F. Fu, L. Shang, Y. Cheng, Z. Gu, Y. Zhao, *Adv. Mater.* **2017**, *29*, 1605765.
[30] J. Guo, Y. Yu, D. Zhang, H. Zhang, Y. Zhao, *Research* **2021**, *2021*, 7065907.
[31] Y. Tian, P. Zhu, X. Tang, C. Zhou, J. Wang, T. Kong, M. Xu, L. Wang, *Nat. Commun.* **2017**, *8*, 1080.
[32] L. Shang, F. Fu, Y. Cheng, Y. Yu, J. Wang, Z. Gu, Y. Zhao, *Small* **2017**, *13*, 1600286.
[33] L. Shang, Y. Wang, Y. Yu, J. Wang, Z. Zhao, H. Xu, Y. Zhao, *J. Mater. Chem. A* **2017**, *5*, 15026.
[34] Y. Liu, N. Yang, X. Li, J. Li, W. Pei, Y. Xu, Y. Hou, Y. Zheng, *Small* **2020**, *16*, 1901819.
[35] R. Shi, Y. Tian, P. Zhu, X. Tang, X. Tian, C. Zhou, L. Wang, *ACS Appl. Mater. Interfaces* **2020**, *12*, 29747.
[36] R. Xie, P. Xu, Y. Liu, L. Li, G. Luo, M. Ding, Q. Liang, *Adv. Mater.* **2018**, *30*, 1705082.
[37] P. Zhu, R. Chen, C. Zhou, Y. Tian, L. Wang, *Chem. Eng. J.* **2021**, *415*, 128944.
[38] Y. Chen, L. Wang, Y. Xue, L. Jiang, Y. Zheng, *Sci. Rep.* **2013**, *3*, 2927.